Supporting Information

Selection of single-atom for surface charge modulation to promote CO_2 activation and stabilize *COOH intermediate for solar fuels

Chih-Yang Huang[a, b,c], Ying-Ren Lai[c,d], Yi-Fan Huang[e], Tsai-Yu Lin[a,b,c], Kongpop Limwatcharagul[a,b,c], Mengstu Etay Ashebir[c, f, g, h, i], Heng-Liang Wu[c,d,j], Michitoshi Hayashi[c,d], Mohammad Qorbani[k, l]*, Kuei-Hsien Chen[c, i]* and Li-Chyong Chen[c, d, m]**

[a]International Graduate Program of Molecular Science and Technology, National Taiwan University (NTU-MST), Taipei 10617, Taiwan
[b]Molecular Science and Technology Program, Taiwan International Graduate Program (TIGP), Academia Sinica, Taipei 11529, Taiwan
[c]Center for Condensed Matter Sciences, National Taiwan University, Taipei 10617, Taiwan
[d]Center of Atomic Initiative for New Materials, National Taiwan University, Taipei, 10617, Taiwan
[e]Department of Mechanical Engineering, National Chin-Yi University of Technology, Taichung 411030, Taiwan
[f]Sustainable Chemical Science and Technology, Taiwan International Graduate Program, Academia Sinica, Nankang, Taipei 11529, Taiwan
[g]Institute of Chemistry, Academia Sinica, Nankang, Taipei 11529, Taiwan
[h]Department of Applied Chemistry, National Yang Ming Chiao Tung University, Hsinchu, 30010, Taiwan
[i]Institute of Atomic and Molecular Sciences, Academia Sinica, Taipei 10617, Taiwan
[j]Department of Chemistry, National Taiwan University, Taipei 10617, Taiwan
[k]Undergraduate Program of Electro-Optical Engineering, National Taiwan Normal University, Taipei 11677, Taiwan
[l]Institute of Electro-Optical Engineering, National Taiwan Normal University, Taipei 11677, Taiwan
[m]Department of Physics, National Taiwan University, Taipei 10617, Taiwan
E-mail: atmyh@ntu.edu.tw; qorbani@ntnu.edu.tw; chenkh@pub.iams.sinica.edu.tw; chenlc@ntu.edu.tw
* Author to whom correspondence should be addressed.

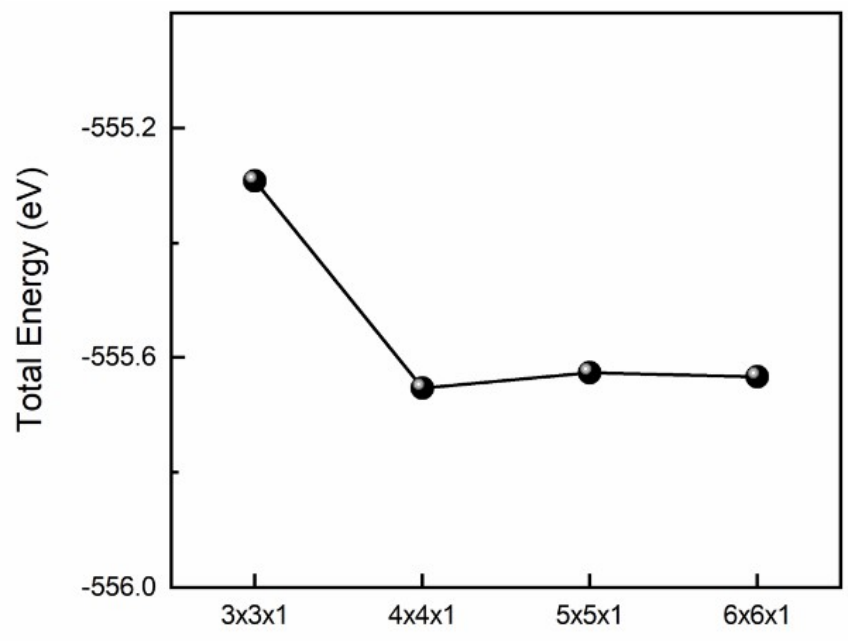

Fig. S1. k-point convergence test. Total energy versus k-point.

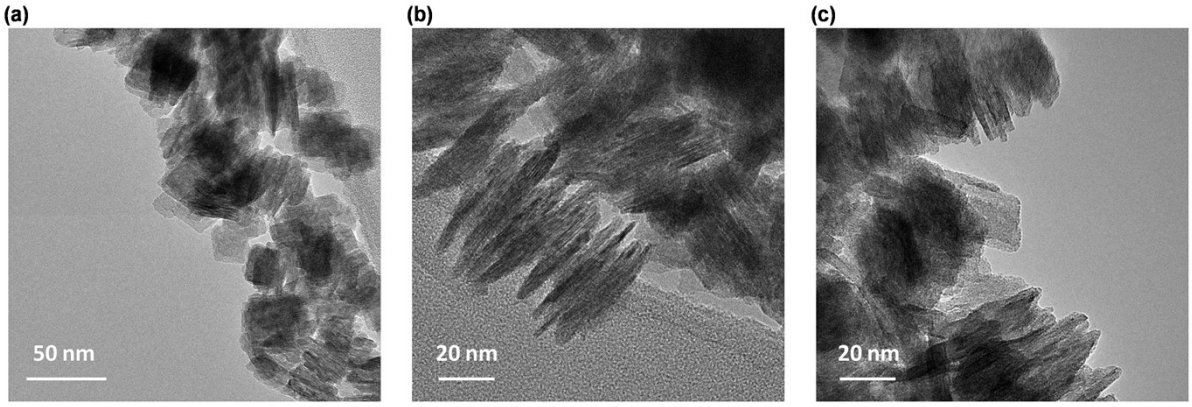

Fig. S2. Microstructure. STEM images of (a) WO_3, (b) SA-Cr-WO_3 and (c) SA-Ni-WO_3

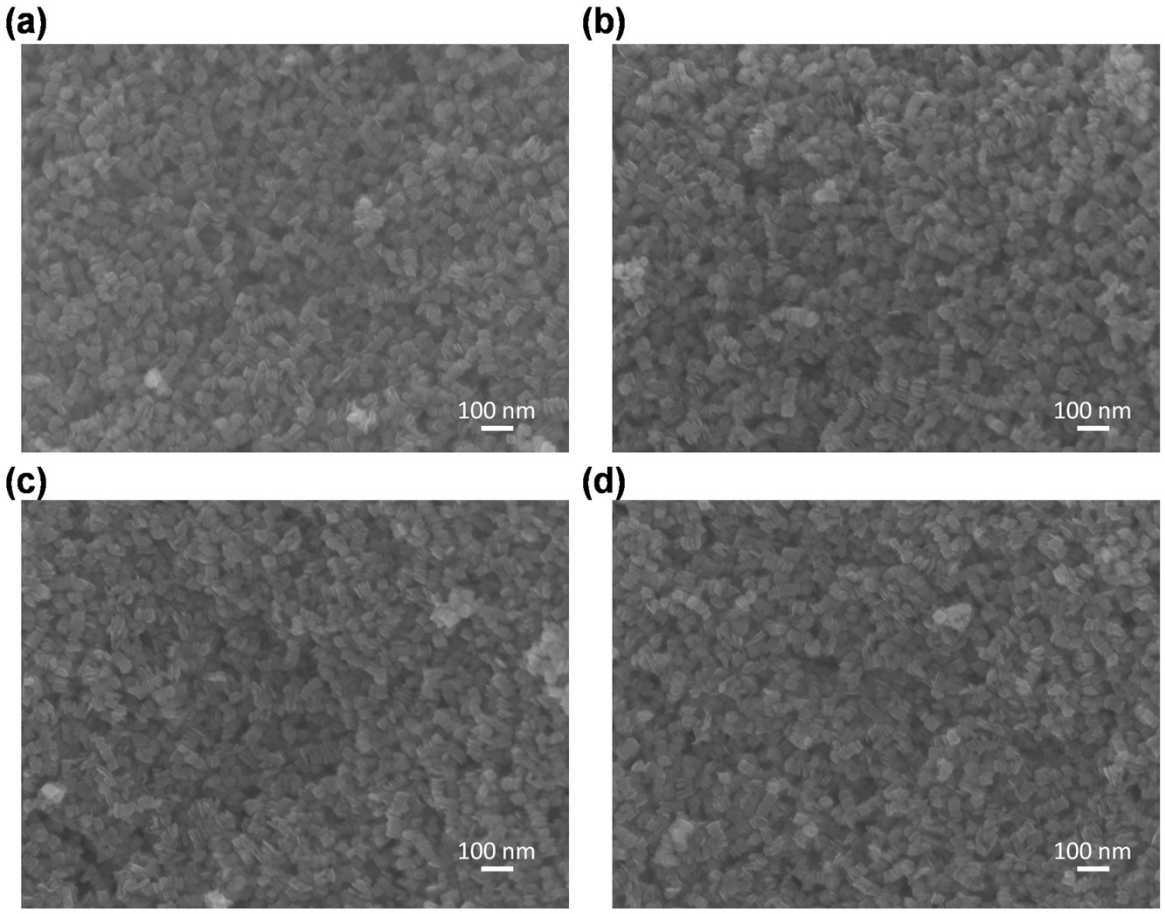

Fig. S3. Morphology. SEM images of (a) WO_3, (b) SA-Cr-WO_3, (c) SA-Fe-WO_3 and (d) SA-Ni-WO_3.

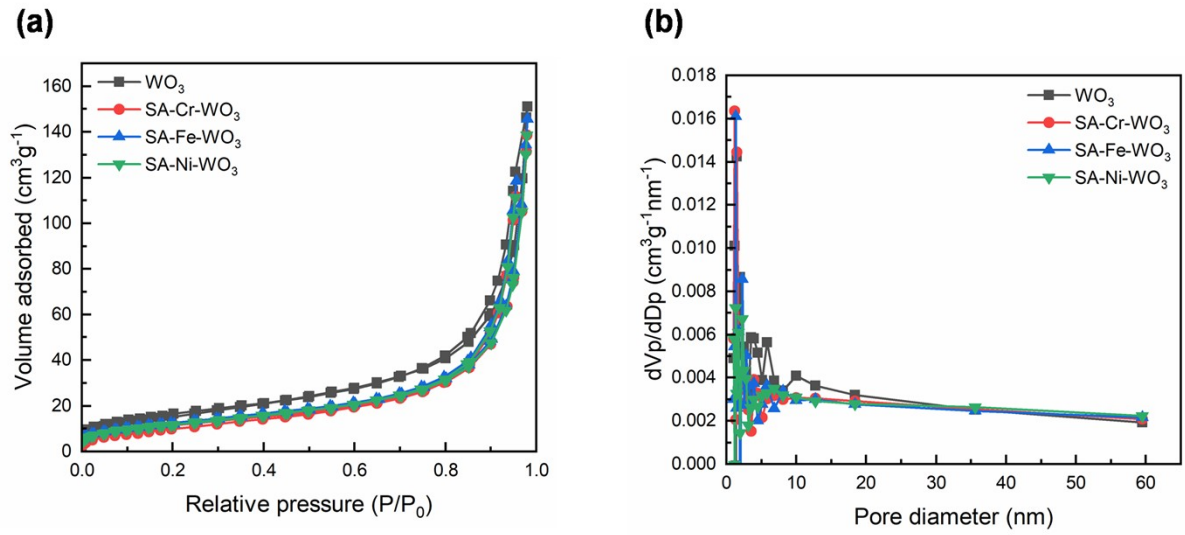

Fig. S4. Surface area analysis of the photocatalyst. (a) Nitrogen adsorption–desorption isotherms and (b) pore size distribution of WO_3, SA-Cr-WO_3, SA-Fe-WO_3, and SA-Ni-WO_3.

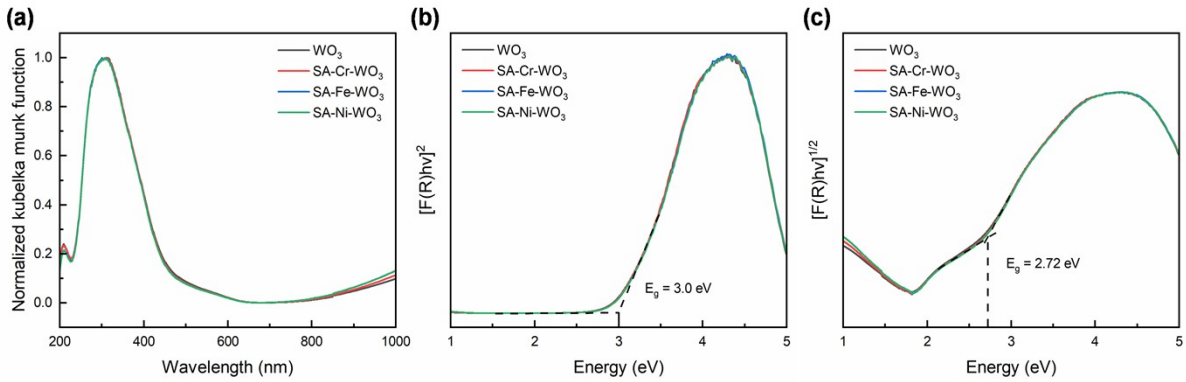

Fig. S5. Optical absorption of photocatalyst. (a) diffuse reflectance spectroscopy spectra. (b, c) Indirect and direct bandgap estimations, respectively.

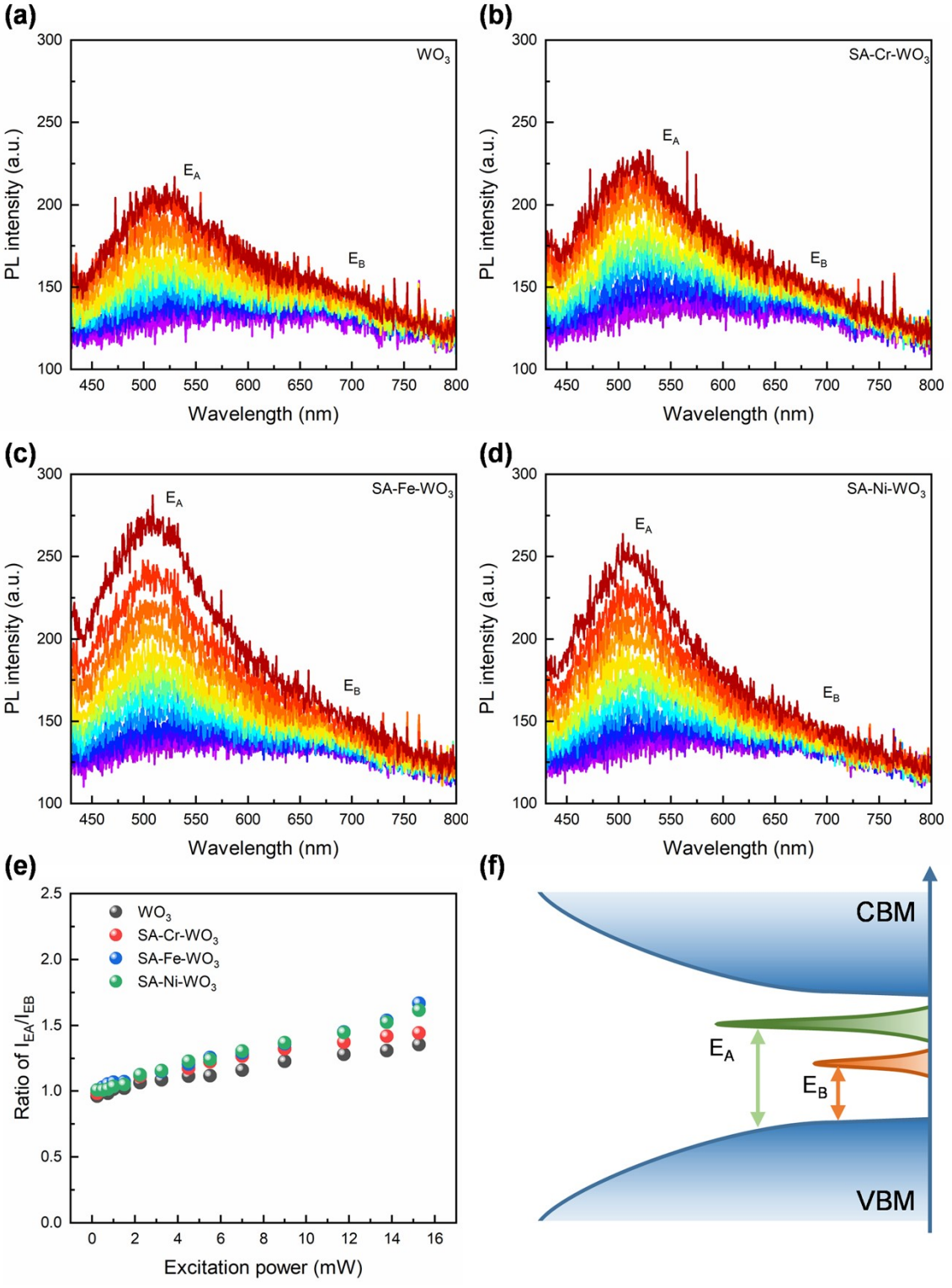

Fig. S6. Power-dependent photoluminescence analysis of WO_3 and transition metal-anchored WO_3. Photoluminescence spectra of (a) WO_3, (b) SA-Cr-WO_3, (c) SA-Fe-WO_3, and (d) SA-Ni-WO_3 under excitation powers ranging from 0.25 to 15.25 mW. (e) Intensity ratio of emission peaks E_A and E_B as a function of excitation power. (f) Schematic illustration of photoluminescence emission in WO_3.

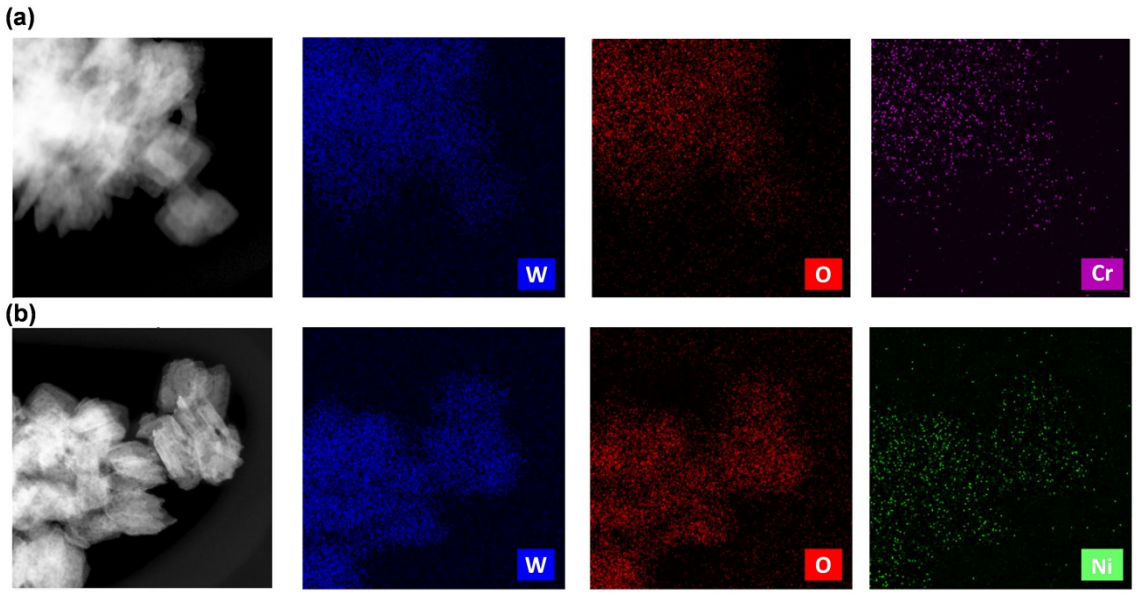

Fig. S7. Distribution of elements. EDS elemental mapping images of (a, b) SA-Cr-WO_3 and SA-Ni-WO_3, respectively.

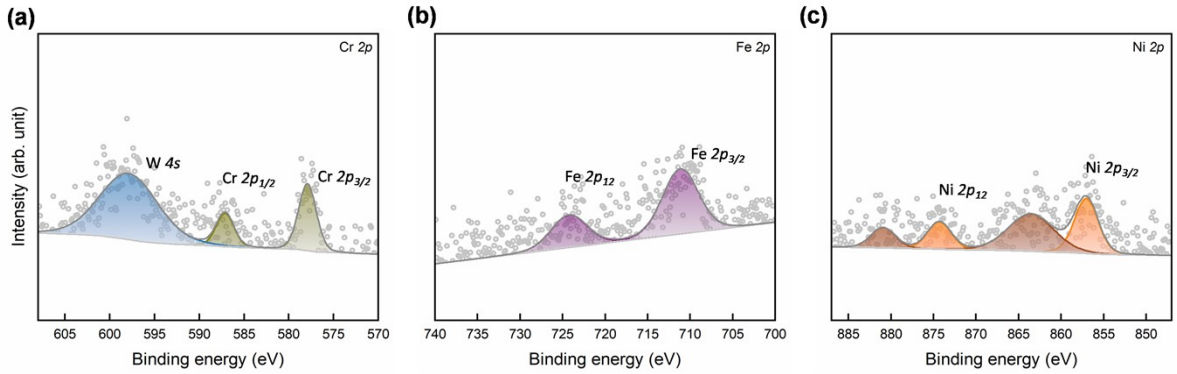

Fig. S8. XPS of transition metal-anchored WO_3. XPS of (a) SA-Cr-WO_3, (b) SA-Fe-WO_3 and (c) SA-Ni-WO_3

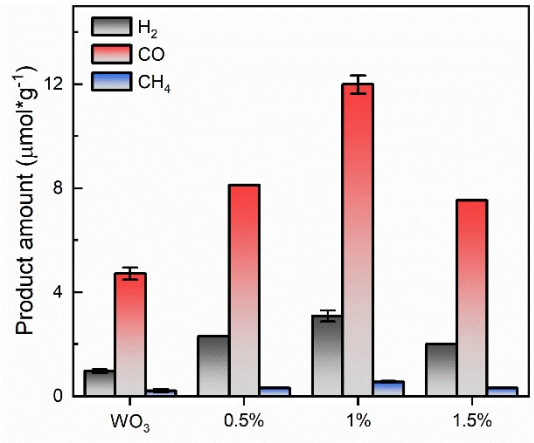

Fig. S9. Optimization of the Fe loading amount for photocatalytic CO_2 reduction. Photocatalytic CO_2 reduction performance of SA-Fe-WO_3 with various Fe loading concentrations (0–1.5%) for an irradiation time of 4 h.

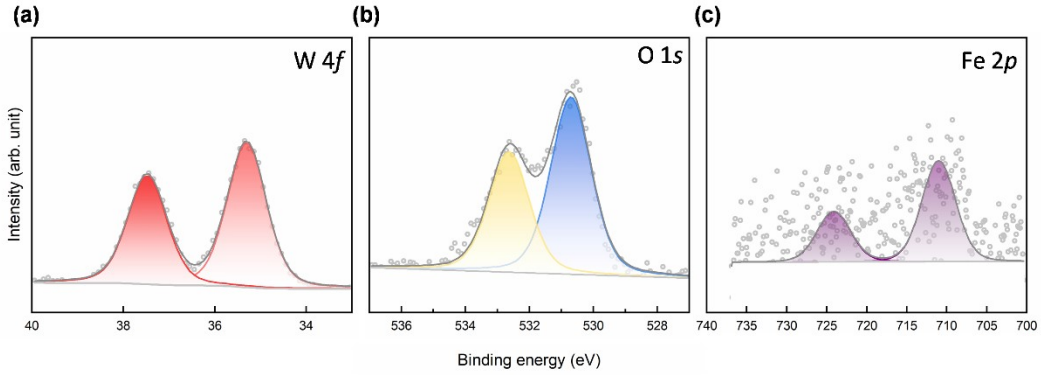

Fig. S10. XPS analysis at high Fe loading. High-resolution XPS spectra of (a) W 4*f*, (b) O 1*s*, and (c) Fe 2*p* for the 1.5% Fe-WO_3 sample.

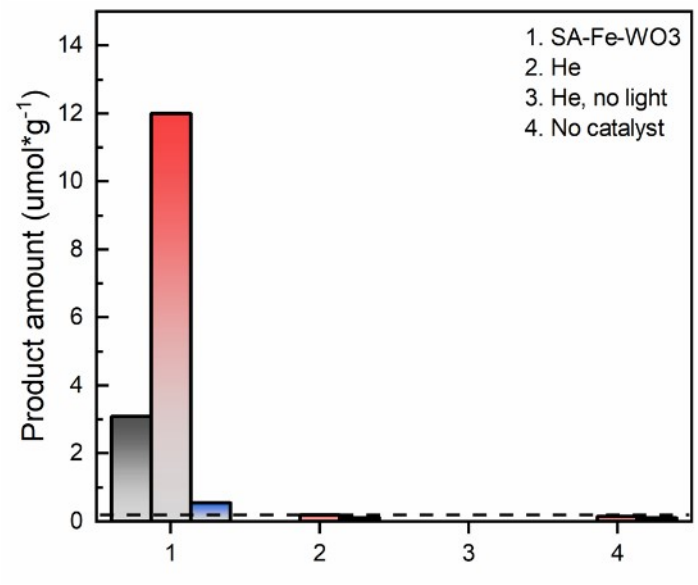

Fig. S11. Blank tests. Blank tests of PC-CO_2RR for SA-Fe-WO_3.

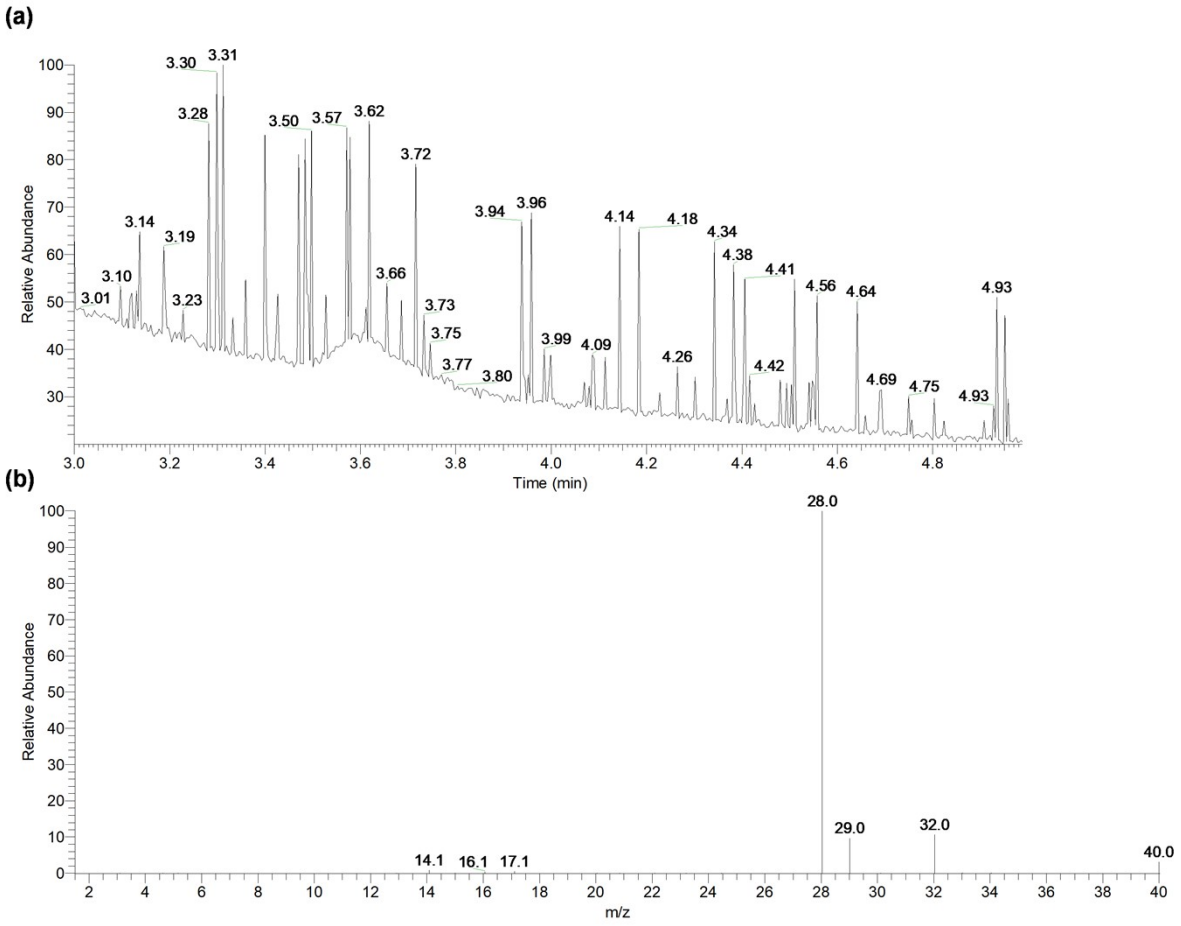

Fig. S12. Isotope tracing analysis of CO_2 photoreduction over SA-Fe-WO_3. (a) Total ion chromatography and (b) mass spectrum of ^{13}C isotope tracing measurement.

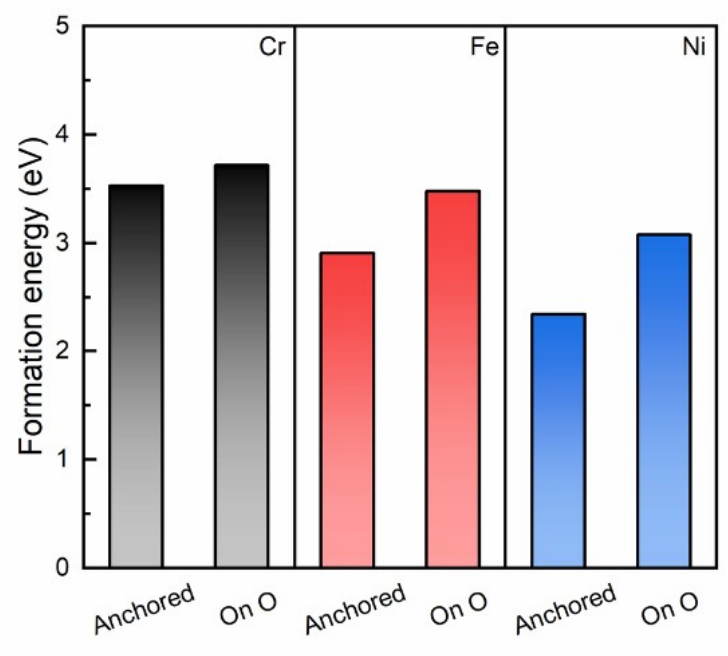

Fig. S13. Formation energy of anchored metals. Calculated formation energy for two possible anchoring configurations for Cr, Fe, and Ni anchored atoms.

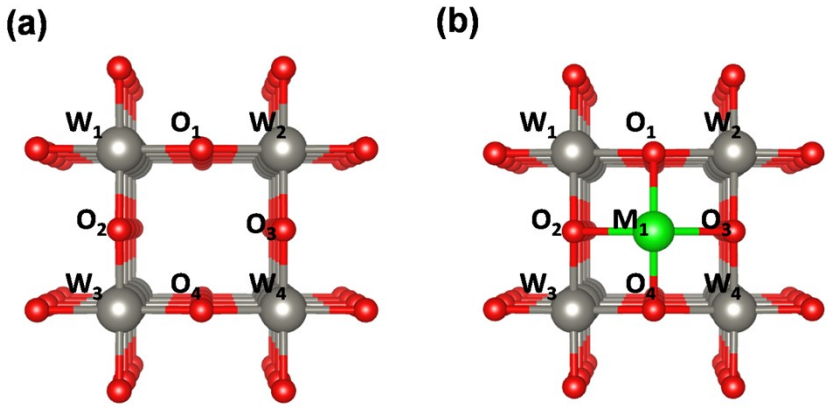

Fig. S14. Schematic illustration of the simulation model. (a, b) WO_3 structure and SA-M-WO_3 structure, respectively. Red: oxygen atom. Grey: tungsten atom. Green: anchored transition metal.

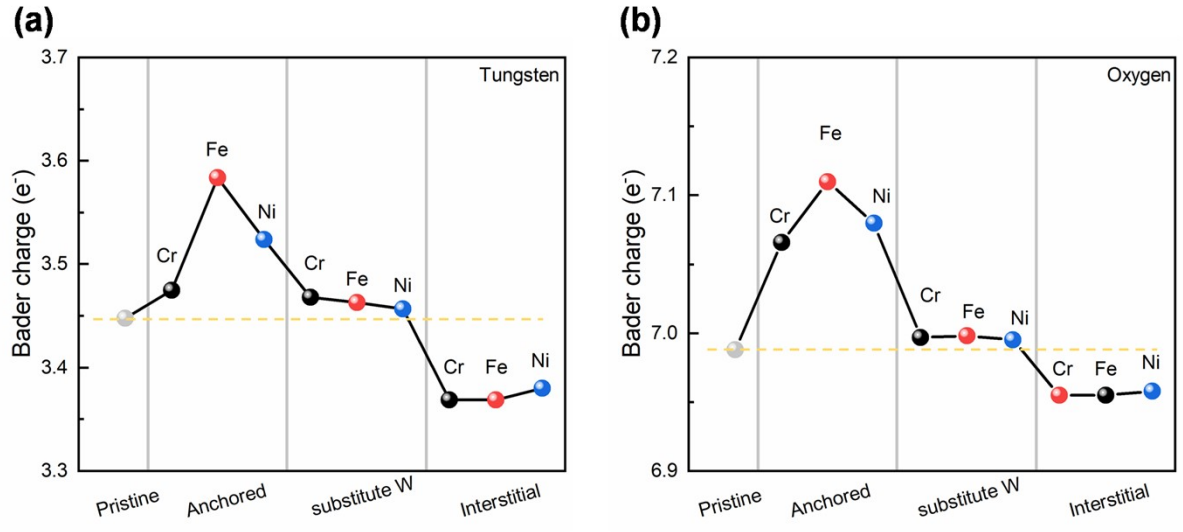

Fig. S15. Bader charge analysis of surface W and O atoms with dopants positioned at various sites. (a, b) Bader charge on tungsten and oxygen atoms, respectively.

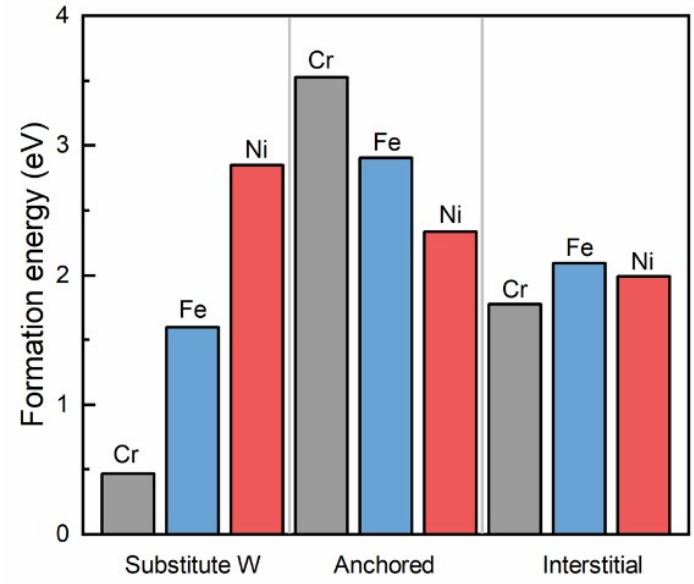

Fig. S16. Formation energy of metals at different positions on WO_3. Calculated formation energy of metals at various positions within the WO_3 lattice, including surface anchoring, substitutional, and interstitial sites

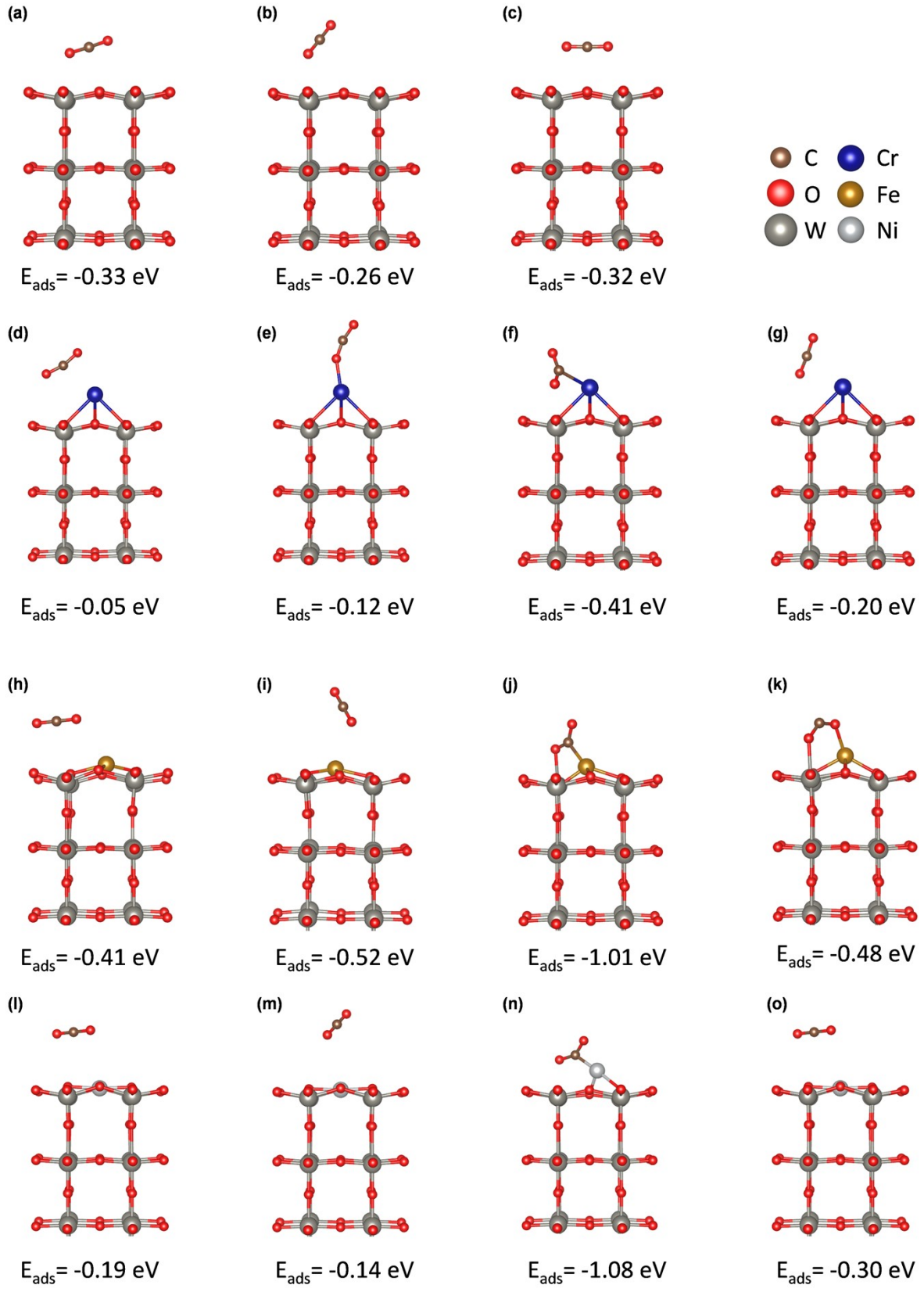

Fig. S17. CO_2 adsorption models on different WO_3 surfaces. CO_2 on (a to c) WO_3, (d to g) SA-Cr-WO_3, (h to k) SA-Fe-WO_3, and (l to o) SA-Ni-WO_3. C, O, W, Cr, Fe and Ni atoms are represented as dark brown, red, dark gray, blue, brown and bone color, respectively

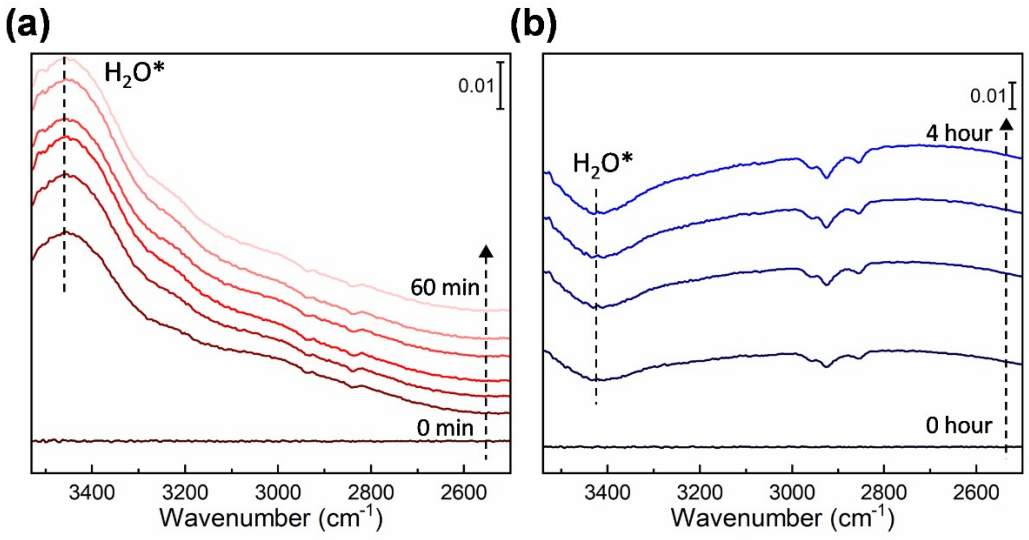

Fig. S18. In-situ FTIR measurements. In-situ FTIR spectra of SA-Fe-WO_3 recorded in H_2O and CO_2 atmospheres under (a) dark conditions and (b) light irradiation.

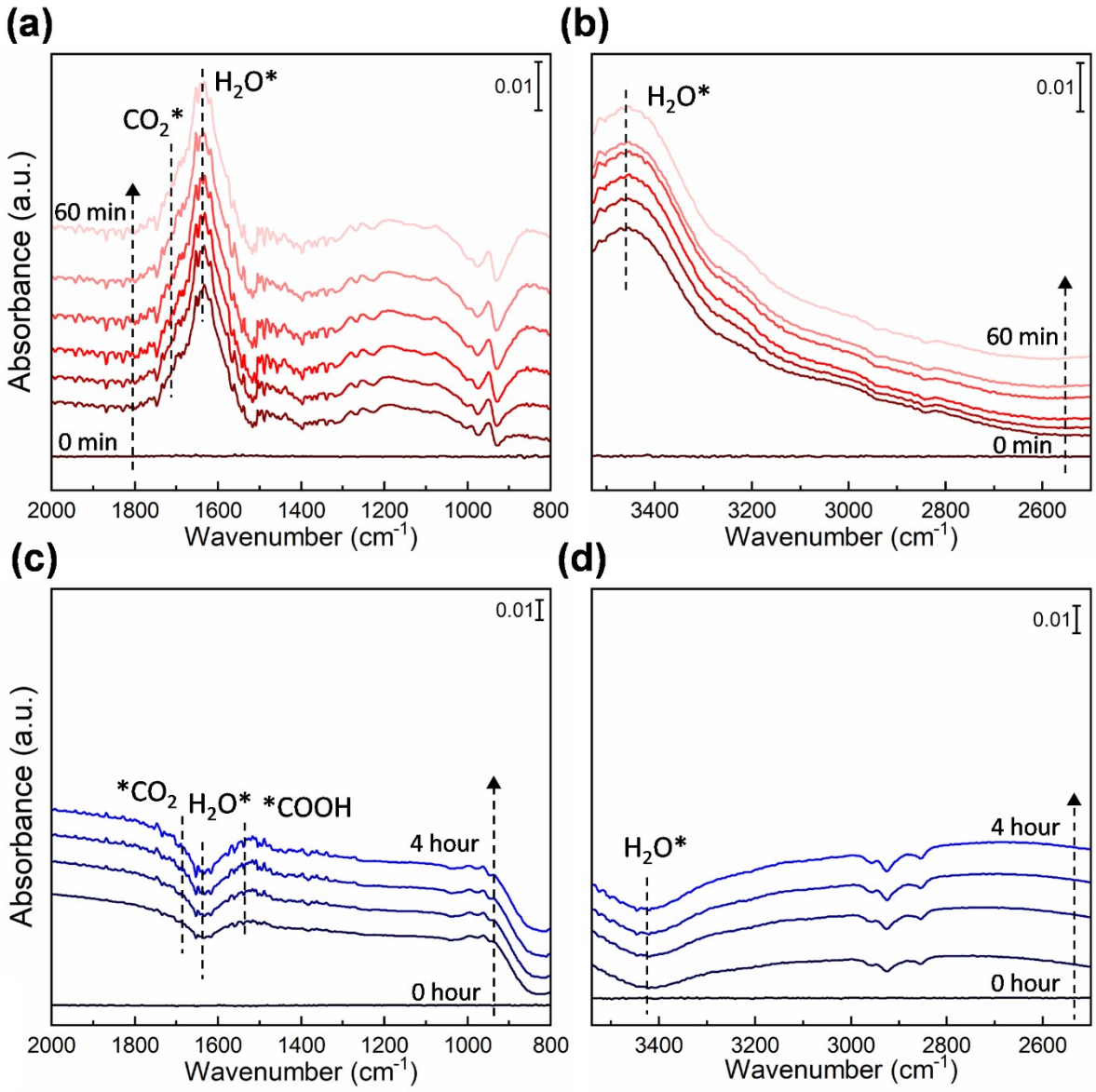

Fig. S19. In-situ FTIR measurements. In-situ FTIR spectra of WO_3 recorded in H_2O and CO_2 atmospheres under (a, b) dark conditions and (c, d) light irradiation.

Table S1. Concentration of the loaded metals. Metal loadings in SA-M-WO_3 (M=Cr, Fe and Ni) measured by ICP-OES. Dopant level was calculated at M/(M+W+O).

Sample	W (at%)	Metal (at%)	Dopant level (at%)
SA-Cr-WO_3	96.9	3.1	0.77
SA-Fe-WO_3	96.7	3.3	0.83
SA-Ni-WO_3	96.1	3.9	0.97

Table S2. Bond length and coordination number. EXAFS fitting parameters of transition metal anchored WO_3.

Sample	Path	CN (N*S0^2)[a]	$R + \Delta R$(Å)[b]	R factor[c]
SA-Cr-WO_3	Cr–O	3.08	1.96	0.0222
SA-Fe-WO_3	Fe–O	4.27	1.99	0.0027
SA-Ni-WO_3	Ni–O	5.16	2.04	0.0138

[a]Coordination number. [b]Bond distance. [c] Least-squares residual for the EXAFS fitting, where typical values are below 0.02. Smaller residual values indicate better fitting accuracy.

Table S3. O–to–W ratio before and after metal anchoring. O–to–W ratios measured by XPS.

Sample	O *1s* (peak area)	W *4f* (peak area)	RSF-corrected O–to–W ratio
WO_3	924.7	1450.6	3.2
SA-Cr-WO_3	1031.2	661.2	3.2
SA-Fe-WO_3	1254.6	791.6	3.1
SA-Ni-WO_3	1164.9	726.9	3.1

Table S4. Bader charge analysis[a]. Bader charge distribution on W and O atoms.

Atom	WO_3	SA-Cr-WO_3	SA-Mn-WO_3	SA-Fe-WO_3	SA-Co-WO_3	SA-Ni-WO_3
W_1	3.448	3.475	3.586	3.584	3.534	3.524
W_2	3.448	3.475	3.586	3.584	3.534	3.524
W_3	3.448	3.475	3.586	3.584	3.535	3.524
W_4	3.448	3.475	3.586	3.584	3.534	3.524
O_1	6.988	7.066	7.140	7.110	7.100	7.080
O_2	6.988	7.066	7.140	7.110	7.100	7.080
O_3	6.988	7.066	7.140	7.110	7.100	7.080
O_4	6.988	7.066	7.140	7.110	7.100	7.080
M_1 (Cr/Fe/Ni)	–	5.556	5.787	6.970	8.163	9.272

[a]W_{1-4} and O_{1-4} represent the tungsten and oxygen atoms surrounding the anchored transition metal. The (Unit: e^-)

Table S5. Bader charge analysis of surface atoms upon –OH anchoring. Calculated Bader charge distribution for W, O and Fe atoms on WO_3 and SA-Fe-WO_3 surface before and after surface hydroxylation.

Atom	WO_3	OH-WO_3	SA-Fe-WO_3	SA-Fe-OH-WO_3
W_1	3.448	3.400	3.584	3.507
W_2	3.448	3.332	3.584	3.491
W_3	3.448	3.392	3.584	3.544
W_4	3.448	3.395	3.584	3.503
O_1	6.988	6.967	7.110	7.044
O_2	6.988	6.988	7.110	7.119
O_3	6.988	6.963	7.110	7.054
O_4	6.988	6.990	7.110	7.115
Fe	–	–	6.970	6.793

Table S6. Structural and electronic properties of CO_2 adsorption on different surfaces. Bond length of C-O_1, C-O_2, angle of O-C-O, adsorption energy and Bader charge of CO_2 molecule adsorbed on the different surfaces.

Sample	d_{C-O1} (Å)	d_{C-O2} (Å)	$\angle_{O-C-O}$ (deg.)	E_{ads} (eV)	Bader charge |e⁻|			
					C	O_2	O_1	CO_2
Free CO_2	1.18	1.18	180.0	0.00	1.91	7.05	7.05	0.00
WO_3	1.17	1.18	178.1	−0.33	1.84	7.09	7.08	0.01
SA-Cr-WO_3	1.24	1.21	144.4	−0.41	2.37	7.04	7.11	0.52
SA-Mn-WO3	1.25	1.26	140.6	-1.26	2.51	7.07	7.13	0.71
SA-Fe-WO_3	1.23	1.29	135.6	−1.01	2.52	7.10	7.06	0.69
SA-Fe-WO_3 (O-down)	1.25	1.26	132.1	−0.48	2.41	7.15	7.18	0.74
SA-Co-WO3	1.22	1.30	133.2	-1.29	2.48	7.06	7.09	0.64
SA-Ni-WO_3	1.25	1.24	144.3	−1.08	2.43	7.02	7.09	0.53

Table S7. Impact of –OH on CO_2 adsorption. Adsorption energy of CO_2 on different surface

Samples	E_{ads} (eV)
WO_3	-0.33
OH-WO_3	-0.40
SA-Fe-WO_3	-1.01
SA-Fe-OH-WO_3	-0.78

Table S8. Gibbs free energy calculation. Calculated Gibbs free energies for the photoreduction of CO_2 to CO over WO_3, SA-Cr-WO_3, SA-Fe-WO_3, and SA-Ni-WO_3. All units are in eV.

Sample	ΔG (*+CO_2)	ΔG (*COOH)	ΔG (*CO+H_2O)	ΔG (*CO)	ΔG (*+CO)
WO_3	0	1.50	0.65	-	0.73
SA-Cr-WO_3	0	-0.55	-0.03	-0.26	0.73
SA-Fe-WO_3	0	-1.73	-1.41	-1.04	0.73
SA-Ni-WO_3	0	-0.47	-0.83	-1.11	0.73

Table S9. Gibbs free energy corrections for gas-phase species. Thermodynamic corrections applied to gas molecules used in Gibbs free energy calculations. All units are in eV.

Species	E_{DFT}	ZPE	TΔS	$\Delta U_{(0\rightarrow T)}$	PV
H_2	-6.77	0.27	0.41	0.06	0.03
CO	-14.78	0.13	0.61	0.06	0.03
CO_2	-22.97	0.31	0.67	0.07	0.03
H_2O	-14.23	0.57	0.59	0.08	0.03

Table S10. Gibbs free energy corrections for WO_3. Thermodynamic corrections applied to adsorbates used in Gibbs free energy calculations. All units are in eV.

WO_3	E_{DFT}	ZPE	TΔS	$\Delta H_{(0\rightarrow T)}$
*	-555.63	-	-	-
*CO_2	-578.90	0.32	0.21	0.09
*COOH	-581.47	0.79	0.19	0.10
CO+H_2O	-585.67	0.83	0.34	0.15
*CO	-	-	-	-

Table S11. Gibbs free energy corrections for SA-Cr-WO_3. Thermodynamic corrections applied to adsorbates used in Gibbs free energy calculations. All units are in eV.

SA-Cr-WO_3	E_{DFT}	ZPE	TΔS	$\Delta H_{(0\rightarrow T)}$
*	-562.02	-	-	-
*CO_2	-585.38	0.29	0.22	0.11
*COOH	-589.72	0.62	0.20	0.10
*CO+H_2O	-592.68	0.78	0.35	0.16
*CO	-578.34	0.18	0.06	0.04
*COH	-580.43	0.44	0.11	0.06
*CHO	-581.77	0.32	0.19	0.09

Table S12. Gibbs free energy corrections for SA-Fe-WO_3. Thermodynamic corrections applied to adsorbates used in Gibbs free energy calculations. All units are in eV.

SA-Fe-WO_3	E_{DFT}	ZPE	TΔS	$\Delta H_{(0\rightarrow T)}$
*	-561.27	-	-	-
*CO_2	-585.23	0.34	0.28	0.14
*COOH	-590.06	0.60	0.35	0.17
*CO+H_2O	-593.54	1.00	0.40	0.21
*CO	-578.34	0.25	0.24	0.11
*COH	-580.30	0.45	0.17	0.07
*CHO	-581.68	0.42	0.16	0.07

Table S13. Gibbs free energy corrections for SA-Ni-WO_3. Thermodynamic corrections applied to adsorbates used in Gibbs free energy calculations. All units are in eV.

SA-Ni-WO_3	E_{DFT}	ZPE	TΔS	$\Delta H_{(0\rightarrow T)}$
*	-559.06	-	-	-
*CO_2	-583.08	0.37	0.25	0.13
*COOH	-586.73	0.69	0.26	0.13
*CO+H_2O	-590.56	0.84	0.39	0.18
*CO	-576.18	0.25	0.26	0.12
*COH	-577.34	0.45	0.20	0.09
*CHO	-578.30	0.43	0.22	0.09

Table S14. Structural and electronic properties of COOH adsorption on different surfaces. Bond length of C-O, C-OH, angle of O-C-OH, Bader charge of COOH, adsorption energy of CO_2 molecule adsorbed on the different surfaces.

Sample	d_{C-O} (Å)	d_{C-OH} (Å)	$\angle_{O-C-OH}$ (deg.)	E_{ads} (eV)	Bader charge COOH|e^-|
WO_3	1.24	1.34	125.25	0.51	0.47
SA-Cr-WO_3	1.21	1.51	115.27	-1.35	1.62
SA-Ni-WO_3	1.27	1.35	115.75	-1.32	1.49